May we remark that this area is in its infancy and much more work is required before a complete strategy for attacking large problems is at hand. The computer will not have its full impact on process design until such a strategy evolves.

ACKNOWLEDGMENT

This study was supported in part by the National Science Foundation.

LITERATURE CITED

1. Cavett, R. H., paper presented at A.I.Ch.E. Pittsburgh meeting (May 19, 1964).
2. Lee, W., J. H. Christensen, and D. F. Rudd, *A.I.Ch.E. J.*, **12**, No. 6, 1104-1110 (1966).
3. Norman, R. L., *ibid.*, **11**, 450 (1965).
4. Rubin, D. I., *Chem. Eng. Progr. Symposium Ser.*, No. 37, **58**, 54 (1962).
5. Steward, D. V., *J. S.I.A.M.*, **2B**, No. 2, 345 (1965).

Manuscript received February 11, 1966; revision received May 26, 1966; paper accepted May 31, 1966.

Heat Transfer and Frost Formation Inside a Liquid Nitrogen-Cooled Tube

R. C. REID, P. L. T. BRIAN, and M. E. WEBER

Massachusetts Institute of Technology, Cambridge, Massachusetts

An experimental study was undertaken of simultaneous heat transfer and frost deposition inside a liquid nitrogen-cooled tube for a range of humidities and Reynolds numbers. The data indicate that diffusion of water vapor within the frost layer caused the frost density and thermal conductivity to increase with time. The increase was so great that the heat transfer rate became constant even while frost continued to accumulate. In a separate study the thermal conductivities of frosts formed on a cryogenic surface were measured and found to be lower than values near the freezing point of water.

Processes in which heat is transferred to a refrigerated surface with the simultaneous deposition of a frost layer are important in refrigeration, freeze-out purification of gases, cryopumping, and the storage of cryogenic liquids. Frost will form on a refrigerated surface that has a temperature below the dew point of the gas and the freezing point of the vapor. For small wall-gas temperature differences, water vapor reaches the wall by molecular and turbulent diffusional processes, and the standard correlations can be used to predict the heat transfer and frost accumulation rates (*1* to *13*). For large temperature differences, however, fog may form in the gas, and the impingement and trapping of fog particles on the surface may become the dominant mechanism of frost deposition. At the present time a rigorous analysis of this mechanism is not possible, although the conditions necessary for fog formation have been studied by Johnstone (*14*).

In natural convection to spherical and cylindrical liquid oxygen tanks (*15, 16*), the frost accumulation rate was only 10 to 30% of the predicted mass transfer rate because of the formation of a fog in the boundary layer flowing past the tank surface. In forced convection to cryogenically cooled cylinders, however, the frost accumulation rates were nearly equal to the predicted rates (*17, 18*). In both natural and forced convection frosting on cryogenic surfaces, the heat transfer rate decreased to a constant value when the air dew point was below 32°F. (liquid water could not condense on the frost surface).

The prediction of heat transfer rate with frosting on cryogenic surfaces is uncertain, not only because of the complex deposition mechanism, but also because of the scarcity of frost density and thermal conductivity data. The present experimental study was undertaken to determine the effect of a frost deposit on heat transfer inside a liquid nitrogen-cooled tube. Attention was focused upon the frost deposition rate and the effect of the frost layer on the heat transfer rate. The humidities studied were in the range where fog formation was important but where liquid water condensation could not occur. In addition, low-temperature frost thermal conductivity data were obtained for a range of frost densities typical of forced convection.

APPARATUS AND PROCEDURE

A cross section of the tubular heat exchanger is shown in Figure 1. A nitrogen-water vapor mixture flowed downward through the central tube (tube *D*), 0.62-in. I.D. and 44.5 diameters long. It was cooled externally by boiling liquid nitrogen. Frost formation occurred on the inside wall. Preceding the exchanger tube was a calming section of the same diameter and 80 diameters long.

The test heat exchanger in Figure 1 was constructed from four concentric copper tubes, the innermost tube being the exchanger tube (tube *D*). The space between tubes *A* and *B* was filled with liquid nitrogen to absorb the heat leak from the surroundings. The space between tubes *B* and *C* contained air. Horizontal plates separated tube *C* into six chambers, which contained the boiling nitrogen required to cool the walls of the exchanger tube. Gravity caused the flow of liquid nitrogen within the chambers, fresh liquid being fed

M. E. Weber is with McGill University, Montreal, Canada.

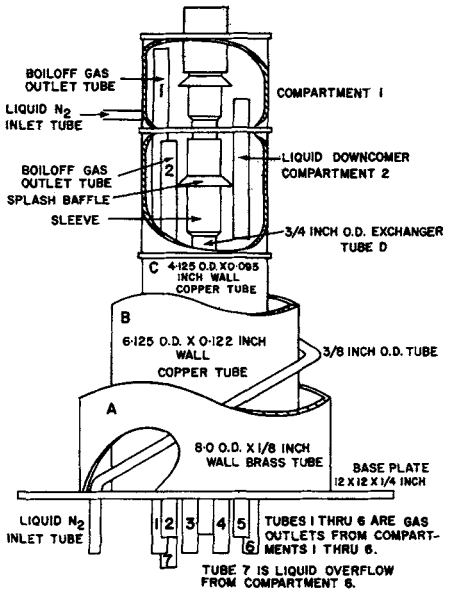

Fig. 1. Heat exchanger cross section.

to the top chamber and the unboiled excess being removed from the bottom chamber. A tubular weir in each compartment maintained a liquid level which sealed the downcomer from the compartment above. The vapor, evolved by heat transfer from the gas flowing through the exchanger tube, was removed separately from each chamber and measured.

The auxiliary apparatus consisted of a supply of dry nitrogen (obtained by boiling liquid nitrogen), a packed tower humidifier, and a preheater to adjust the temperature of the gas entering the test exchanger. The apparatus was arranged so that any fraction of the dry nitrogen could be humidified and remixed with the dry portion to provide the desired humidity.

Gas temperatures and humidities were measured at the exchanger inlet and outlet. The temperature of the gas leaving the exchanger was measured in a sudden expansion in the outlet piping which served as a mixing chamber. A small sample for water vapor analysis was withdrawn continuously downstream from an electrical heater located after the mixing chamber. Therefore, the measured outlet humidity was the total water content (including fog) of the gas leaving the exchanger. Outlet water contents were measured continuously with a commercial phosphorous pentoxide absorption and electrolysis cell. In addition, exchanger pressure drop and compartmental boil-off rates were measured at intervals.

RESULTS

The data are presented in terms of the number of initial velocity heads lost and an apparent overall heat transfer coefficient for the entire tube. The number of velocity heads lost was obtained by dividing the frictional pressure drop by $G_o^2/(2\rho_{G,b}g_c)$. The frictional pressure drop was obtained by correcting the measured pressure drop for the change of momentum of the gas due to the difference in the inlet and outlet exchanger temperatures. This method of expressing the results was used because it facilitates the comparison of different runs by compensating for small differences in inlet temperature and flow rate. For the unfrosted exchanger the number of velocity heads lost is equal to $4f_oL/D_o$.

The apparent overall heat transfer coefficient was calculated from

$$\overline{U_a} = \frac{Wc_p}{\pi D_o L} \ln\left[\frac{T_1 - T_w}{T_2 - T_w}\right] \qquad (1)$$

The wall temperature was −320°F. and the inlet gas temperature was between 55° and 80°F. For the flow of dry gas through the exchanger, Equation (1) yields the true overall heat transfer coefficient, which is essentially equal to the gas film coefficient. For the flow of moist gas the coefficient of Equation (1) is smaller than the overall coefficient for sensible heat transfer because of the release of latent heat as water vapor condenses either in the bulk gas (fog formation) or at the frost surface (vapor transfer to the surface). However, the apparent coefficient of Equation (1) is within 5% of the overall coefficient for sensible heat transfer for inlet humidities less than 0.3 mole %.

Frost-Free Heat Transfer and Friction

Nusselt numbers and friction factors were obtained for the flow of dry nitrogen through the frost-free exchanger. These data were taken in order to test the standard high-temperature correlations for applicability at low temperatures and to provide a basis for comparison of the frosting data. The gas film heat transfer coefficient was correlated within 4% by

$$N_{Nu,f} = 0.021\,(N_{Re,f})^{0.8}(N_{Pr})^{1/3} \qquad (2)$$

for Reynolds numbers between 8,800 and 38,000. Equation (3) is in good agreement with the correlations of McAdams (*19*) and the more recent low temperature data of Hall and Tsao (*20*).

The friction factors for the cooling of nitrogen in the exchanger were correlated within 12% by

$$f_o = 0.00140 + 0.125/(N_{Re,b})^{0.32} \qquad (3)$$

for Reynolds numbers between 6,000 and 30,000 with an average deviation of 5% independent of Reynolds number. Equation (3) is also given by McAdams (*19*) as the best correlation of friction factors in isothermal turbulent flow.

Frosting Heat Transfer and Friction

All frosting runs followed the pattern shown in Figures 2 through 5. The Reynolds numbers in these and subsequent figures are the original film Reynolds numbers, that is, the film Reynolds numbers for the frost-free exchanger with same flow rate and inlet temperature.

In most of the runs part of the frost layer would occasionally shear off the exchanger wall. When this occurred the outlet water content increased suddenly and the pressure drop and outlet temperature decreased suddenly. This occurred, for example, in the run with an inlet humidity of 0.20 mole % after 50 min. For clarity of

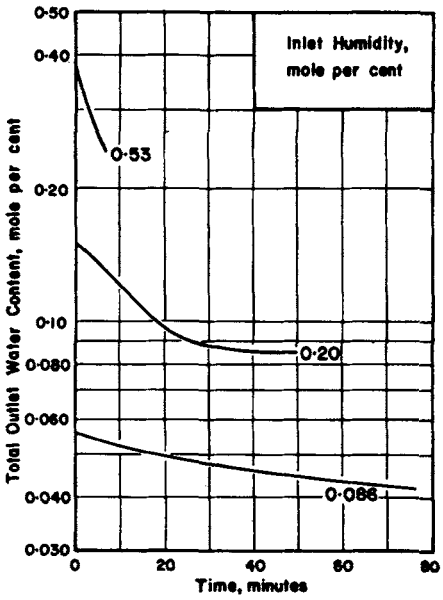

Fig. 2. Total outlet water content for three runs with an original film Reynolds number of 17,500.

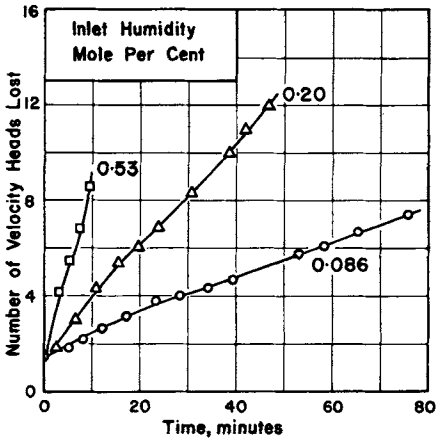

Fig. 3. Frictional head loss across the frosting exchanger (frosted length, 2.3 ft.) for three runs with an original film Reynolds number of 17,500.

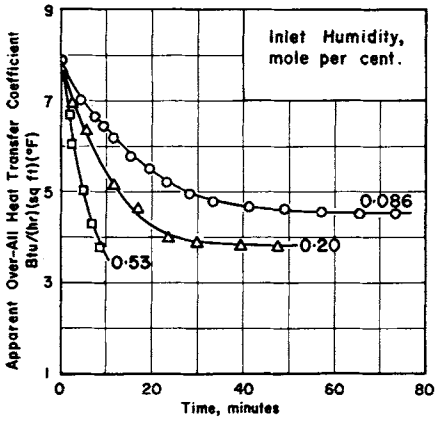

Fig. 4. Apparent overall heat transfer coefficient for the frosting exchanger for three runs with an original film Reynolds number of 17,500.

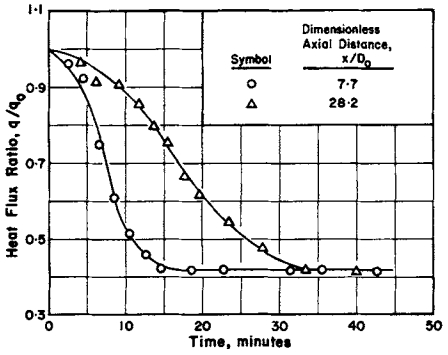

Fig. 5. Local heat flux ratio at two axial locations. Original film Reynolds number, 17,500; inlet humidity, 0.20 mole %.

presentation, the data beyond the time of shearing have been omitted.

DISCUSSION

The essential features of the data are seen by examining the run with an inlet humidity of 0.20 mole % in Figures 2, 3, 4, and 5. The apparent overall heat transfer coefficient decreased for 25 min. and then remained constant, while the frost accumulation and the pressure drop continued to increase. The heat flux decreased more rapidly near the exchanger inlet. For runs less than 25 min. the difference between the heat fluxes for the two locations shown in Figure 5 was larger than that that would be obtained if the frost were distributed uniformly. This result suggests that frost accumulated more rapidly near the front of the exchanger, and that after some time the thermal resistance of the frost layer and the gas film reached a steady state value more quickly where the accumulation rate was larger.

The decrease in gas film resistance because of the blockage of the flow area by the frost was calculated (*21*) to be insufficient to yield a constant heat transfer coefficient with a constant frost density. Therefore, the frost density and thermal conductivity probably increased simultaneously because the frost continued to accumulate at an approximately constant rate over the major portion of a run.

Performance as a Function of Frost Accumulation

Figure 6 presents the ratio of the frictional head loss to the frost-free head loss for two Reynolds numbers and several humidities. The heat transfer results corresponding to the runs presented in Figure 6 are shown in Figure 7 as a dimensionless heat transfer parameter $\bar{\xi}_H$, defined by

$$\bar{\xi}_H = \frac{\bar{U}_a}{c_p G_o} \{N_{Re,\,f,\,o}\}^{0.2} (N_{Pr})^{2/3} \qquad (4)$$

A comparison of the data in these figures for a Reynolds number of 17,500 indicates that the higher humidities probably yielded lower frost densities. Since lower frost densities give lower frost thermal conductivities (see below), this explanation clarifies both the increased frictional head losses for a given frost accumulation and the lower steady state apparent heat transfer coefficients which were observed for the higher inlet humidities.

If the frost is assumed to densify with the passage of time, the dependence of frost density on inlet humidity

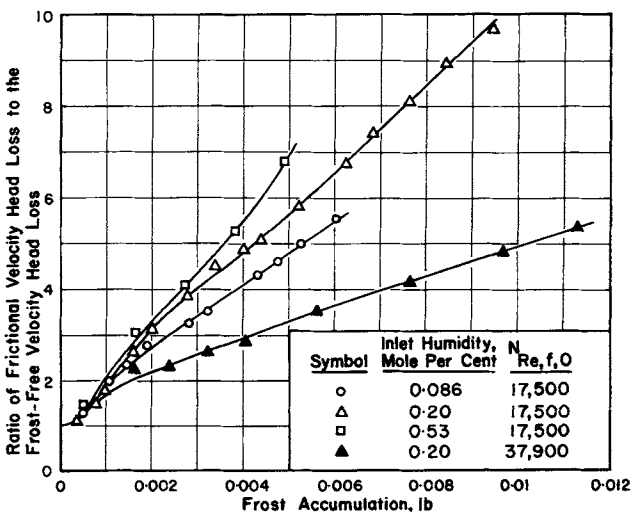

Fig. 6. Velocity head loss ratio vs. frost accumulation.

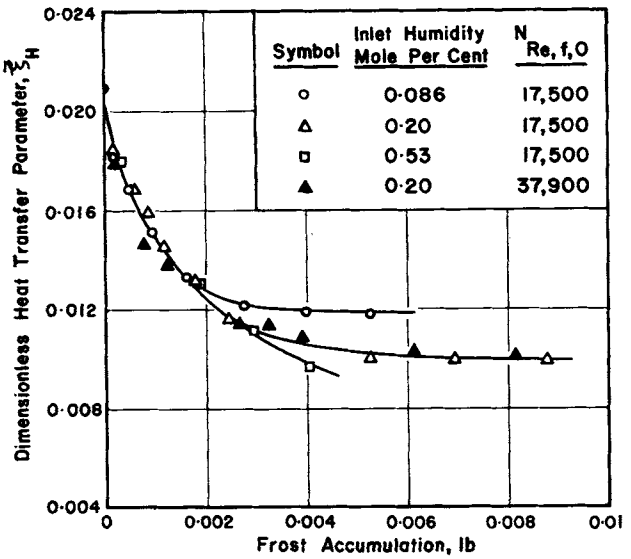

Fig. 7. Dimensionless heat transfer parameter vs. frost accumulation.

may be explained by the longer time required to accumulate a given amount of frost at low inlet humidity. This densification occurs through the diffusion of water vapor within the frost. The temperature gradient across the frost produces a water vapor concentration gradient which causes diffusion toward the cold wall, thus increasing the frost density. Densification by internal diffusion has been observed in frosts on surfaces at higher temperatures (*10*).

The data of Figure 6 at different Reynolds numbers indicate that lower Reynolds numbers gave either less uniform frost profiles or lower frost densities. A calculation (*21*) of the dimensionless heat transfer parameter for several frost densities and frost distributions agreed best with the heat transfer data when it was assumed that the frost distribution was independent of Reynolds number (for Reynolds numbers greater than 9,000), and that the frost density increased not only with time but also with gas flow rate. This is not unreasonable, since the higher gas velocities might throw ice particles toward the wall with higher velocities and pack the frost layer more tightly.

Models of the frost structure and the internal vapor diffusion process are presented below. Due to the sensitivity of the internal diffusion model to the frost-gas interface temperature, it is difficult to make accurate predictions of the heat transfer rates for a long tube. However, the models predict that the overall heat transfer coefficient reaches a constant value and that the higher humidities yield lower steady state coefficients in qualitative agreement with the data.

Frost Deposition Models

Two models which were expected to give the maximum and minimum frost deposition rates were investigated. For the minimum deposition rate (saturation model), fog was assumed to form as soon as the bulk gas reached saturation. All fog was assumed to pass through the exchanger, that is, no deposition of fog particles. The maximum deposition rate was calculated by permitting the gas to become supersaturated under the assumption that no fog formed (supersaturation model). In both models frost deposition was assumed to be by molecular and turbulent diffusion, with the deposition rate given by the product of a mass transfer coefficient and a bulk gas-to-frost surface driving force.

Supersaturation Model. It was assumed that fog did not form, that is, supersaturation occurred. The frost deposition driving force was the difference in partial pressure between the bulk gas and the vapor pressure at the frost surface temperature.

Saturation Model. Fog was assumed to form as soon as the bulk gas became saturated. Additional fog formation as the gas passed through the exchanger maintained the bulk gas at saturation, that is, the fog formation rate was infinitely fast. The mass transfer driving force after saturation was reached was the difference between the vapor pressures at the bulk gas temperature and at the frost surface temperature.

The roughness criterion developed by Chen and Rohsenow (*9*) indicated that for the high Reynolds numbers and low frost thermal conductivities of this work, the frost surface was hydrodynamically smooth. Therefore, the diameter of the frosted tube was used in Equation (2) to calculate the gas film heat transfer coefficient directly and to calculate the mass transfer coefficient through the Chilton-Colburn analogy. A frost density was assumed for the calculation and Figure 9 was used to obtain the thermal conductivity from the assumed value of the density. The frost density values (4 to 10 lb./cu.ft.) used in calculating the surface temperature had a negligible effect on the frost deposition driving force since the water vapor pressures at the frost surface were well below the partial pressures of water vapor in the bulk gas. Therefore, the model deposition rates presented in Figure 8 are essentially independent of the assumed frost properties.

The experimental data given by the solid line in Figure 8 indicate that the rate of frost accumulation increased with time. The rate of frost accumulation predicted by the saturation model increases with time because the point in the exchanger at which the bulk gas reaches saturation moves downstream as the frost insulates the tube wall. For long times both models yield nearly the same frost deposition rates. The experimental data in Figure 8 agree more closely with the saturation model for short times, thus indicating that considerable fog formation may have occurred. For long times, however, the data fall slightly below the models, due perhaps to the effect of frost roughness on the mass transfer coefficient (9).

CONCLUSIONS

The following general picture of frosting has emerged from this work:

1. The heat transfer rate approached a steady state even while frost continued to accumulate.
2. The heat transfer steady state was the result of a simultaneous increase in frost density and thermal conductivity. These increases were probably caused by the

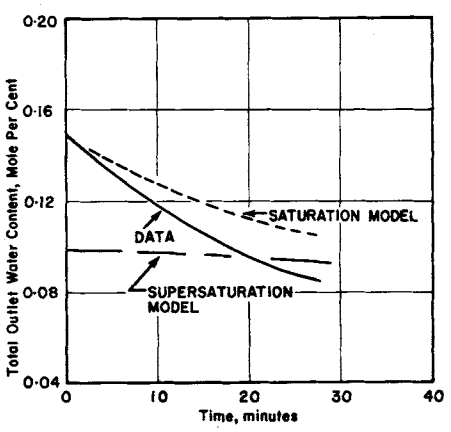

Fig. 8. Comparison of the outlet water content predicted by the frost deposition models with the data for a run with an original film Reynolds number of 17,500 and an inlet humidity of 0.20 mole %.

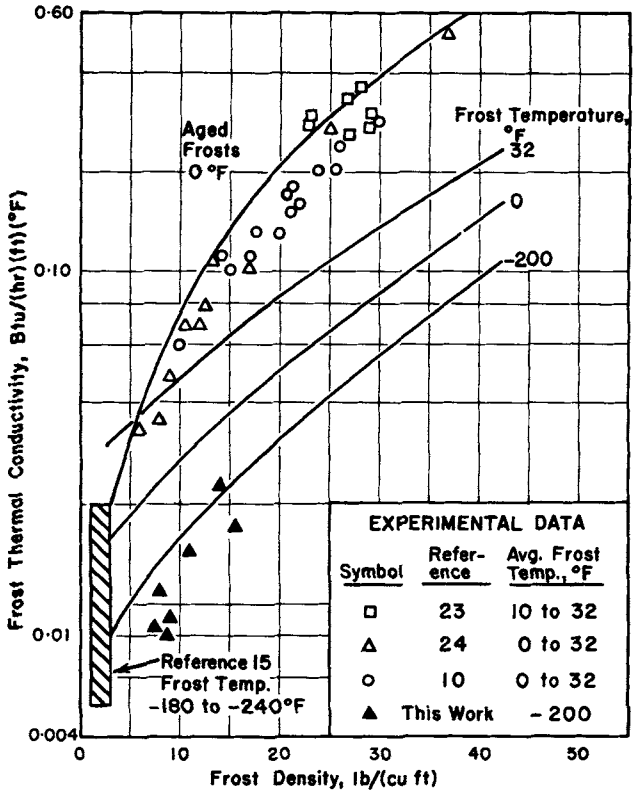

Fig. 9. Frost thermal conductivity-density relationship. This work covered Reynolds numbers between 2,900 and 8,200 and humidities from 0.6 to 1.7 mole %. Other data: forced convection (23), natural snow (24), and natural convection (10, 15). The lines were calculated from the frost structural model.

diffusion of water vapor within the frost toward the cold wall.

3. Lower humidities and higher Reynolds numbers gave denser frost layers for a given frost accumulation.

In addition:

4. The heat transfer parameter was only a function of frost accumulation and inlet humidity for Reynolds numbers above 9,000.

5. The rate of frost accumulation was approximated by two simple frost deposition models.

FROST THERMAL CONDUCTIVITY

Reliable frost thermal conductivities exist over a range of densities only for temperatures between 0° and 32°F. These data and those of Holten (*15*) for low-temperature frosts are shown in Figure 9. Additional data from reference *18* were not included in Figure 9, since the deposits of that study were composed of alternating ice-frost layers caused by the condensation of liquid water on the frost surface. These deposits, which were obtained from high humidity gas streams, were not typical of those obtained here. A complete description of high humidity frosts is presented in reference *17*. It was the purpose of the work reported here to measure the density and thermal conductivity of frosts formed in forced flow over a cryogenic surface, and to formulate a frost model to predict the thermal conductivity.

APPARATUS

The test surface was a refrigerated circular copper plate, approximately 2¼ in. in diameter, set flush in the bottom wall of a thin rectangular duct, ½ in. high by 7 in. wide. The test plate was surrounded by a guard section to absorb the atmospheric heat leak. The test surface was cooled by cylindrical copper fins which were immersed in liquid nitrogen contained in a cylinder below the test surface. The amount of nitrogen boiled in this chamber was a measure of the heat flux to the test plate.

A temperature within the frost was obtained with a thermocouple placed a measured distance above the test surface. This thermocouple was made by bringing 0.005-in. diameter copper and constantan wires through opposite sides of the duct, soldering the junction and stretching the wires taut. Therefore, the wires were parallel to the cooled surface and normal to the direction of flow. For the low frost temperatures of this study the thermocouple error due to radiation was calculated to be less than 1% of the plate-to-thermocouple temperature difference. The frost density was determined by measuring the frost thickness and weighing the frost scraped from a small area.

The auxiliary apparatus consisted of nitrogen tanks, a blower, a packed tower humidifier, and an electric heater to provide a nitrogen stream with a controlled humidity and temperature. The nitrogen boil-off and the thermocouple temperature were measured as functions of time.

RESULTS AND DISCUSSION

Frost Thermal Conductivity

Figure 9 shows that the frost thermal conductivities of this study were well below those for high-temperature frosts with the same density. In both temperature ranges the thermal conductivity increased with increasing density. The curves in Figure 9 were calculated from the frost structural model described in the Appendix.* The model predicts that frost thermal conductivity increases with frost density and temperature in agreement with the data.

The open symbols in Figure 9 are above the 32°F. line calculated from the frost model. This may have been due to structural changes within the frost at high temperatures. The diffusion of water vapor within the frost increases the frost density and thermal conductivity because the dense phase becomes more icelike and the assumptions of the model break down. A calculation (see Appendix) of the thermal conductivity of a frost that has aged in this manner gave the upper curve labeled *Aged Frosts* in Figure 9. Essentially, the same curve was obtained for all temperatures between 0° and 32°F. The model indicates that aging has a greater effect on thermal conductivity than does temperature. Sufficient data are not available to test this prediction.

Heat Transfer and Internal Vapor Diffusion

Figure 10 shows that the heat flux through the test surface decreased to a steady state value similar to the tubular results presented earlier. The lines in the figure were calculated by assuming that the rate of increase of frost thickness was given by the difference between the rate of frost accumulation and the rate of diffusion from the frost surface into the layer, divided by the frost density. The vapor diffusing into the frost layer was assumed to spread uniformly throughout the layer so that there were no density gradients within the frost. The temperature gradient forcing diffusion was taken to be the average temperature gradient across the frost layer. For a flat plate

$$\frac{d\rho_F}{d\theta} = \left[\frac{\rho_F}{m_F}\right]^2 [\beta(T_s)]\,(T_s - T_w)\left(1 - \frac{\rho_F}{\rho_s}\right) \quad (5)$$

where $\beta(T_s)$ is proportional to the slope of the vapor pressure curve and is a strong function of the frost surface temperature, increasing over 100-fold between −60° and +30°F. Calculations (*21*) indicated that for the conditions of the runs made here and in the tubular exchanger,

* Deposited as Document 8746 with the American Documentation Institute Auxiliary Publications Project, Photoduplication Service, Library of Congress, Washington, D. C., and may be obtained for $1.25 for photoprints or 35-mm. microfilm.

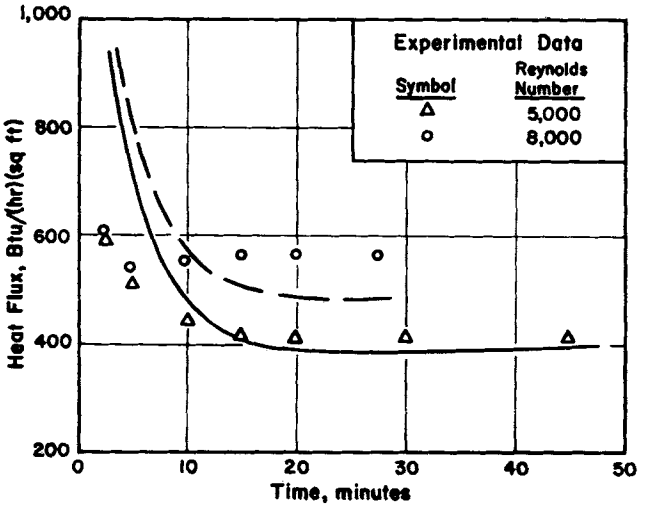

Fig. 10. Variation of the heat flux during frosting. The lines were predicted by the internal diffusion model. The Reynolds numbers are dashed line, 8,000 and solid line, 5,000. The humidity was 1.43 mole %.

the rate of density increase did not become important until the surface temperature was approximately −60°F. Therefore, the overall heat transfer coefficient and frictional pressure loss should have been independent of humidity until the surface temperature became high enough for diffusion within the layer to become important (in qualitative agreement with the data shown in Figures 6 and 7). Stepwise calculations were made of the heat flux by using Equation (5), an initial frost density of 4.0 lb./(cu.ft.), gas film heat transfer coefficients from reference 22, and the assumption that the frost deposition rate was constant at the average value for the run. The frost thermal conductivity was taken from the predictions of the model plotted in Figure 9 for a temperature of −150°F. The predicted lines in Figure 10 are in rough agreement with the data. The model predicts the existence of a constant heat flux for long times.

CONCLUSIONS

1. The thermal conductivity of low temperature frost is considerably lower than that of frost at high temperatures.
2. The frost structural model is in satisfactory agreement with the experimental thermal conductivities.
3. The internal diffusion model and the frost structural model yield heat flux predictions in rough agreement with the data.

ACKNOWLEDGMENT

The authors thank Irving Brazinsky for his assistance in building and operating the flat plate apparatus. This study was made possible by grant National Science Foundation G-14893.

NOTATION

c_p = heat capacity of gas, B.t.u./(lb.)(°F.)
C_T = total concentration, lb.-mole gas and water/cu.ft.
$\mathcal{D}$ = diffusion coefficient, sq.ft./hr.
D_o = diameter of frost-free tube, ft.
f_o = friction factor for frost-free exchanger
G_o = frost-free mass velocity, lb./(hr.)(sq.ft.)
L = exchanger length, ft.
m_F = frost accumulation per unit frost-free area, lb./sq.ft.
M_G = molecular weight of gas
M_v = molecular weight of vapor (water)
N_{Nu} = Nusselt number
N_{Pr} = Prandtl number
N_{Re} = Reynolds number
q = heat flux, B.t.u./(hr.)(sq.ft.)
q_o = frost-free heat flux, B.t.u./(hr.)(sq.ft.)
T_1 = bulk gas temperature at exchanger inlet, °F.
T_2 = bulk gas temperature at exchanger outlet, °F.
T_s = frost surface temperature, °F.
T_w = tube wall temperature, °F.
$\overline{U_a}$ = apparent overall heat transfer coefficient as defined by Equation (1), B.t.u./(hr.)(sq.ft.)(°F.)
W = weight rate of flow of gas, lb./hr.
x = axial distance from exchanger inlet, ft.
Y^s = saturation mole fraction

Greek Letters

$\beta(T_s)$ = diffusion function $= \mathcal{D}\dfrac{M_V C_T}{1-Y^s}\left(\dfrac{dY^s}{dT}\right)_{T_s}$, lb./(hr.(ft.)(°F.)

$\overline{\xi_H}$ = heat transfer parameter as defined by Equation (4)
ρ_s = ice density, lb./cu.ft.
θ = time, hr.

Subscripts

0 = zero time, that is, frost free
b = evaluated at exchanger bulk temperature
f = evaluated at exchanger film temperature

LITERATURE CITED

1. Bailey, B. M., *Advan. Cryogenic Eng.*, **2**, 45-50 (1960).
2. Beatty, K. O., E. B. Finch, and E. M. Schoenborn, *Proc. Gen. Disc. Heat Transfer (London)*, 32-37 (1951).
3. Chung, P. M., and A. B. Algren, *Heating, Piping Air Conditioning*, **30**, No. 9, 171-178; No. 10, 115-22 (1958).
4. Coles, W. D., and R. S. Ruggeri, *Natl. Advisory Committee Aeronaut. Tech. Note 3104* (1954).
5. Han, L. S., S. M. Andrichak, and R. F. Barron, *Am. Soc. Mech. Engr. Paper No. 64-WA/HT9* (1964).
6. Hardy, J. K., K. C. Hales, and G. Mann, *Food Invest. Board Spec. Rept. 54*, Dept. Sci. Ind. Res., H. M. Stationery Office, London (1951).
7. Kamei, S., T. Mizushina, S. Kifune, and T. Koto, *Chem. Eng. (Japan)*, **14**, No. 1, 53-60 (1950).
8. Prins, L., *Kaltetechnik*, **8**, 160-164, 182-186 (1956).
9. Chen, M. M., and W. Rohsenow, *J. Heat Transfer*, **86**, 334-340 (1964).
10. Schropp, K., *Z. Ges. Kalte-Ind.*, **42**, 81-85, 126-131, 151-154 (1935).
11. Whitehurst, C. H., *A.S.H.R.A.E. J.*, **4**, No. 5, 58-69 (1962).
12. Stoecker, W., *Refrig. Eng.*, **65**, No. 2, 42-46 (1957).
13. ———, *Trans. A.S.H.R.A.E.*, **66**, 91-103 (1960).
14. Johnstone, H. F., M. D. Kelley, and D. L. McKinley, *Ind. Eng. Chem.*, **42**, 2298-2303 (1950).
15. Holten, D. C., *Advan. Cryogenic Eng.*, **6**, 499-508 (1961).
16. Ruccia, F. E., and C. M. Mohr, *ibid.*, **4**, 307-318 (1960).
17. Richards, R. J., D. K. Edmonds, and R. B. Jacobs, *Supplement Bull. Inst. Froid* (1962).
18. Smith, R. V., D. K. Edmonds, E. G. F. Brentari, and R. J. Richards, *Advan. Cryogenic Eng.*, **9**, 88-97 (1964).
19. McAdams, W. H., "Heat Transmission," 3 ed., pp. 155-219, McGraw-Hill, New York (1954).
20. Hall, T. A., and P. H. Tsao, *Proc. Roy. Soc.*, **A191**, 6-21 (1947).
21. Weber, M. E., Sc.D. thesis, Massachusetts Inst. Technol., Cambridge (1964).
22. Kays, W. M., and A. L. London, "Compact Heat Exchangers," Figure 32, McGraw-Hill, New York (1958).
23. Coles, W. D., *Natl. Advisory Committee Aeronaut. Tech. Note 3143* (1954).
24. Devaux, J., *Ann. Phys.*, **20**, No. 10, 5-67 (1933).

Manuscript received December 9, 1964; revision received June 13, 1966; paper accepted June 14, 1966.